Bioactive Materials 6 (2021) 3244–3253

Contents lists available at ScienceDirect

Bioactive Materials

journal homepage: www.sciencedirect.com/journal/bioactive-materials

Dendrimer-decorated nanogels: Efficient nanocarriers for biodistribution *in vivo* and chemotherapy of ovarian carcinoma

Xin Li [a,b], Zhijun Ouyang [c], Helin Li [a,b], Chaolei Hu [a,b], Pabitra Saha [a], Lingxi Xing [e,**], Xiangyang Shi [c,d,***], Andrij Pich [a,b,f,*]

[a] DWI-Leibniz-Institute for Interactive Materials e.V, 52056, Aachen, Germany
[b] Institute for Technical and Macromolecular Chemistry, RWTH Aachen University, 52074, Aachen, Germany
[c] College of Chemistry, Chemical Engineering and Biotechnology, Donghua University, Shanghai, 201620, China
[d] CQM-Centro de Química da Madeira, Universidade da Madeira, Campus da Penteada, 9000-390, Funchal, Portugal
[e] Department of Gynecology and Obstetrics, XinHua Hospital, School of Medicine, Shanghai Jiao Tong University, Shanghai, 200092, China
[f] Aachen Maastricht Institute for Biobased Materials, Maastricht University, NL-6167 RD, Geleen, the Netherlands

ARTICLE INFO

Keywords:
Nanogels
Dendrimer
Surface charge
Thermal/pH dual-responsiveness
Drug delivery

ABSTRACT

Nanomedicine has revolutionized disease theranostics by the accurate diagnosis and efficient therapy. Here, the PAMAM dendrimer decorated PVCL-GMA nanogels (NGs) were developed for favorable biodistribution *in vivo* and enhanced antitumor efficacy of ovarian carcinoma. By an ingenious design, the NGs with a unique structure that GMA-rich domains were localized on the surface were synthesized *via* precipitation polymerization. After G2 dendrimer decoration, the overall charge is changed from neutral to positive, and the NGs-G2 display the whole charge nature of positively charged corona and neutral core. Importantly, the unique architecture and charge conversion of NGs-G2 have a profound impact on the biodistribution and drug delivery *in vivo*. As a consequence of this alteration, the NGs-G2 as nanocarriers emerge the highly sought biodistribution of reduced liver accumulation, enhanced tumor uptake, and promoted drug release, resulting in the significantly augmented antitumor efficacy with low side effects. Remarkably, this finding is contrary to some reported work that the nanocarriers with positive charge have preferential liver uptake. Moreover, the NGs-G2 also displayed thermal/pH dual-responsive behaviors, excellent biocompatibility, improved cellular uptake, and stimuli-responsive drug release. Encouragingly, this work demonstrates a novel insight into the strategy for optimizing design, improving biodistribution and enhancing theranostic efficacy of nanocarriers.

1. Introduction

Over the past few decades, the development of nanomedicine has revolutionized disease management *via* highly specific targeting or recognition, precision diagnosis, efficient treatment, and real-time monitoring [1–4]. However, the sophisticated biological environments in the body impose considerable barriers to the transport of cargoes for the targeted regions [5,6]. The ovarian carcinoma, especially, having the highest mortality rate in gynecological cancers, is difficult to theranostics drawing support from nanoplatforms due to its dense extracellular matrix [7,8]. In recent years, some novel nanocarriers have been designed by optimizing their physicochemical properties, such as size, softness, shape, surface charge and modification, to achieve highly efficient delivery, to improve theranostic efficacy and reduce systemic toxicity [9–13].

A 3D cross-linked polymer colloids, nanogels (NGs) as nanocarriers have attracted much attention in biomedical applications, including drug/enzyme delivery, images and therapy of tumors, due to their unique properties [14–16]. All the time we explored various NGs that having the controllable size, deformable softness, highly porous network, excellent biocompatibility and stimuli-responsiveness can be employed as functional nanocarriers for improved tumor theranostics

Peer review under responsibility of KeAi Communications Co., Ltd.
* Corresponding author. DWI-Leibniz-Institute for Interactive Materials e.V, 52056, Aachen, Germany.
** Corresponding author.
*** Corresponding author. College of Chemistry, Chemical Engineering and Biotechnology, Donghua University, 201620, Shanghai, China.
E-mail addresses: xinglingxi@xinhuamed.com.cn (L. Xing), xshi@dhu.edu.cn (X. Shi), pich@dwi.rwth-aachen.de (A. Pich).

https://doi.org/10.1016/j.bioactmat.2021.02.031
Received 16 December 2020; Received in revised form 23 February 2021; Accepted 25 February 2021

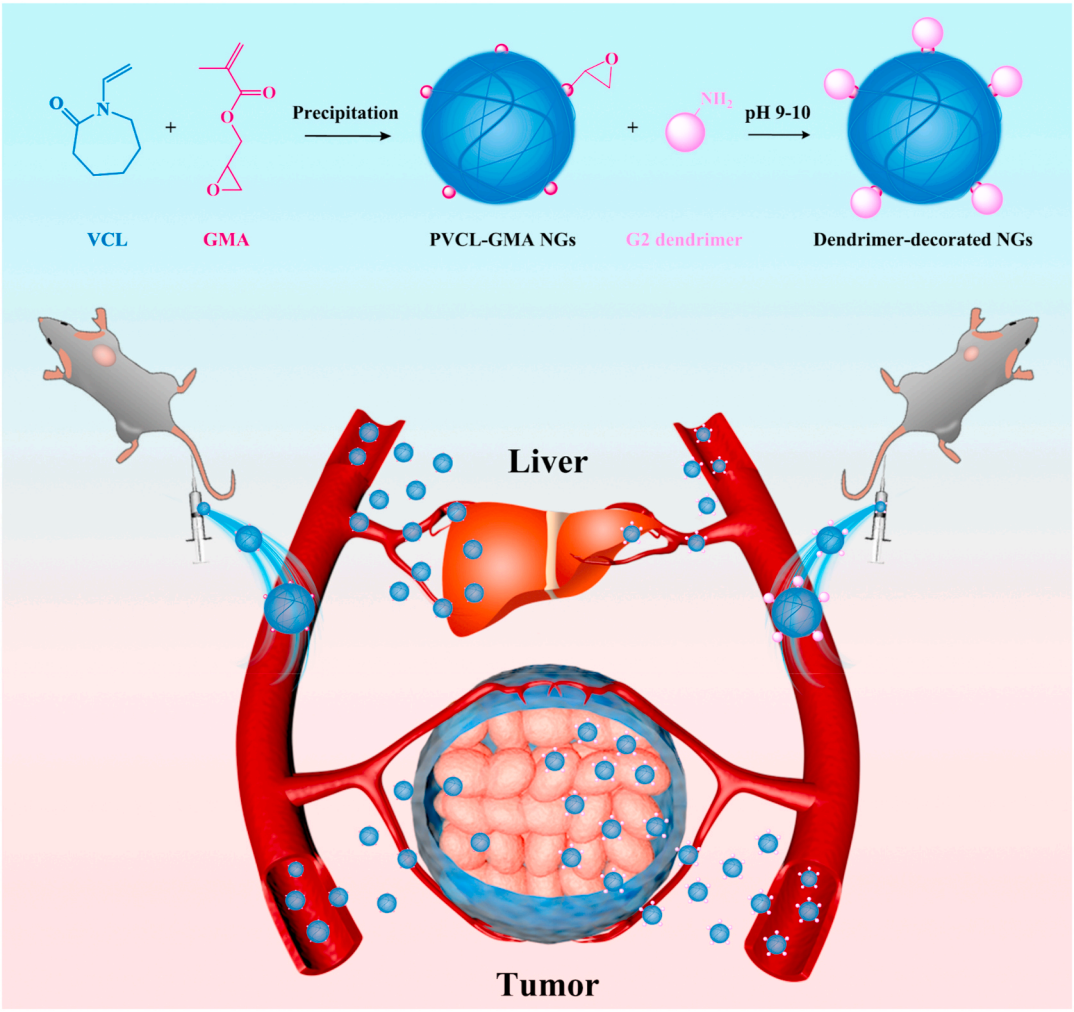

Scheme 1. Schematic illustration of the preparation of dendrimer-decorated PVCL-GMA NGs (NGs-G2) for efficient drug delivery *in vivo*. Compared to PVCL-GMA NGs, the NGs-G2 display elevated tumor accumulation, reduced liver uptake, and more efficient antitumor activity due to their whole charge nature of positively charged corona and neutral core.

[17–25]. In particular, the biocompatible PVCL-based NGs exist a volume phase transition temperature (VPTT) of about 35 °C which is close to body temperature, and high cargo loading capacity along with enhanced tumor accumulation for biomedical purposes [26–28]. Despite all that, these NGs also display low tissue penetration, insufficient cellular internalization and high liver retention, which seriously limit their further clinical translation.

Additionally, the poly(amidoamine) (PAMAM) dendrimers with the properties of well-defined structural architecture, highly branch and multivalent cooperativity have been extensively utilized in the biomedical fields [29–32]. In particular, the easily modifiable surface, ultrasmall size, and strong cationic characteristic render PAMAM dendrimers as effective nanocarriers to increase the bioavailability of hydrophobic molecules and improve the permeability within tumors [33,34]. The PAMAM dendrimers can encapsulate or modify various functional elements to form stable nanoplatforms with the cationic surface, active diffusion, and good cell membrane affinity, resulting in facilitating tissue penetration and cellular internalization [35,36].

It is well known that the nanocarriers with different morphologies, amphipathy, sizes, charges, and modifications obviously impact their biodistribution and tumor accumulation *in vivo* [37–41]. Remarkably, in very recent work, Shen et al. [42,43] synthesized enzyme-responsive polymer or dendrimer-drug conjugation for enhanced tumor penetration *via* active transport of endocytosis and transcytosis to extend the therapeutic efficacy of pancreatic cancer. The cationic character of these nanocarriers can significantly improve treatment efficacy. Moreover, Chan et al. [44] evidenced that the dominant mechanism regarding the entry of nanoplatforms into tumors is active transportation instead of passive diffusion. Therefore, we hypothesized that the cationic dendrimer decorated on the surface of NGs could reduce the unfavorable liver retention and augment tumor accumulation of NGs.

The multicellular spheroid penetration and/or cellular internalization of PVCL-based NGs with different sizes and dendrimer-crosslinked alginate NGs with negative charge have been investigated [27,45]. However, these works only explored the capability of cell permeation and uptake for NGs *in vitro*, which could not reflect the distribution and tumor accumulation *in vivo* due to the sophisticated biological environments. For the clinical translation of nanomedicines, it is necessary to evaluate the *in vivo* behavior of novel NGs. Herein, for the first time, we developed the dendrimer decorated PVCL-GMA NGs for biodistribution *in vivo* and enhanced antitumor efficacy of ovarian carcinoma (Scheme 1). The NGs with adjustable size were first synthesized by precipitation polymerization, and the GMA-rich domains were localized on the surface of NGs in the form of small clumps. Subsequently, G2 dendrimer with different contents was conjugated on the surface of NGs by the reaction with GMA. After dendrimer decoration, the formed NGs-G2 display good colloidal stability, thermal/pH dual-responsive behaviors, excellent biocompatibility, improved cellular uptake, stimuli-responsive drug release, and elevated anticancer activity. More importantly, the decoration of G2 on the surface of NGs significantly

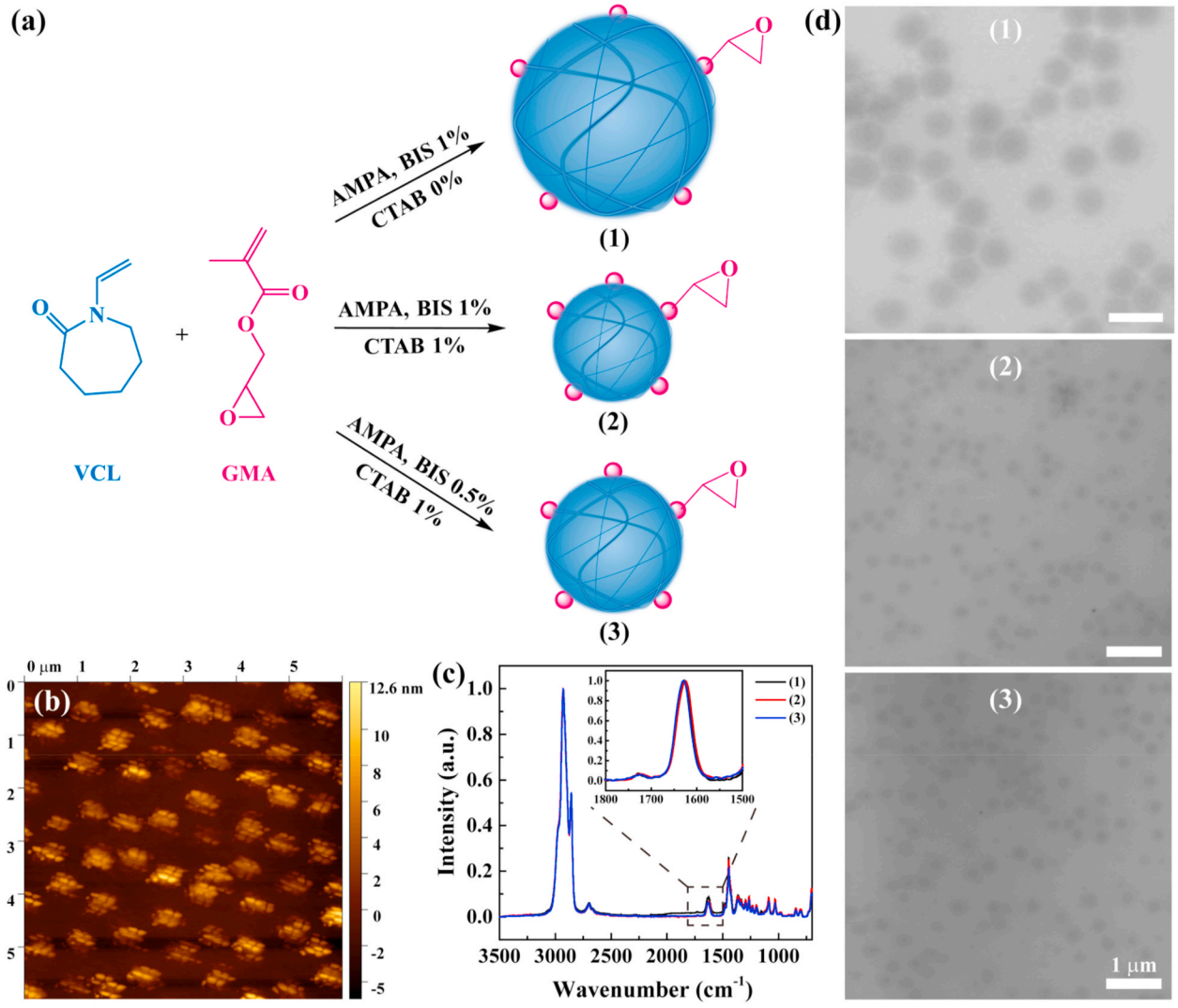

Fig. 1. (a) Schematic synthesis of PVCL-GMA NGs with different diameters. (b) AFM image of PVCL-GMA NGs of (2). (c) Raman spectra and (d) TEM images of PVCL-GMA NGs of (1), (2) and (3). (1), (2) and (3) represent the PVCL-GMA NGs (BIS 1%, CTAB 0%), PVCL-GMA NGs (BIS 1%, CTAB 1%) and PVCL-GMA NGs (BIS 0.5%, CTAB 1%), respectively.

affects the surface charge (from neutral to positive). As a consequence, compared to free NGs, the NGs-G2 show the elevated cellular internalization, promoted drug release, and reduced liver uptake, leading to highly favorable biodistribution and antitumor efficacy. Notably, some literatures imply that the positively charged nanoplatforms prefer to accumulate in the liver after intravenous injection [46–49]. However, our results clearly illustrate that the nanocarriers possessing overall positively charged corona with neutral core could result in the reduced liver uptake and enhanced antitumor efficacy with low side effects *in vivo*.

2. Results and discussion

2.1. Synthesis and characterization of PVCL-GMA NGs and NGs-G2

To obtain the NGs with adjustable size, narrow size distribution and biocompatibility, we used the precipitation polymerization method (Fig. 1a). The PVCL-GMA NGs were synthesized using monomers of *N*-vinylcaprolactam (VCL) and glycidyl methacrylate (GMA), the initiator 2,2′-Azobis(2-methylpropionamidine)dihydro-chloride (AMPA), the crosslinker *N*,*N*′-Methylenebis(acrylamide) (BIS), and the surfactant cetyltrimethylammonium bromide (CTAB). The GMA (10 mol%) was added after the initiation of polymerization to ensure the localization of epoxy groups on the surface of NGs [50]. This increases the accessibility of epoxy groups, which can be used for further conjugation of different functional molecules like protein, drugs, targeted agents, or fluorescent dyes. Atomic force microscopy (AFM) images (Fig. 1b) indicated that the GMA-rich domains are localized on the surface of NGs in the form of small clumps instead of even distribution. Also, the incorporation of GMA in NGs was demonstrated by Fourier transform infrared (FTIR) spectroscopy (Fig. S1). The characteristic peaks at 1618 and 1723 cm^{-1} were the carbonyl vibration from VCL and GMA, respectively. To analyze quantitatively the GMA contents in NGs, the Raman spectroscopy was used (Fig. 1c). The absorption peaks of the carbonyl group at 1623 cm^{-1} and 1729 cm^{-1} for VCL and GMA respectively were selected as representative signals for the monomer units in the copolymer structure. Using the mixtures of linear PGMA and PVCL homopolymers, the calibration curve was designed (Fig. S2). Furthermore, the actual GMA contents in these NGs were calculated to be 9.0–9.2 mol%, which is in consistent with the theoretical GMA content of 10 mol% (Fig. S3).

Additionally, the size of NGs can be controlled by adjusting the contents of BIS and CTAB. Transmission electron microscopy (TEM) and Cryo-field emission scanning electron microscopy (Cryo-FESEM) images revealed that these three NGs had spherical shape, and the NGs (1), NGs

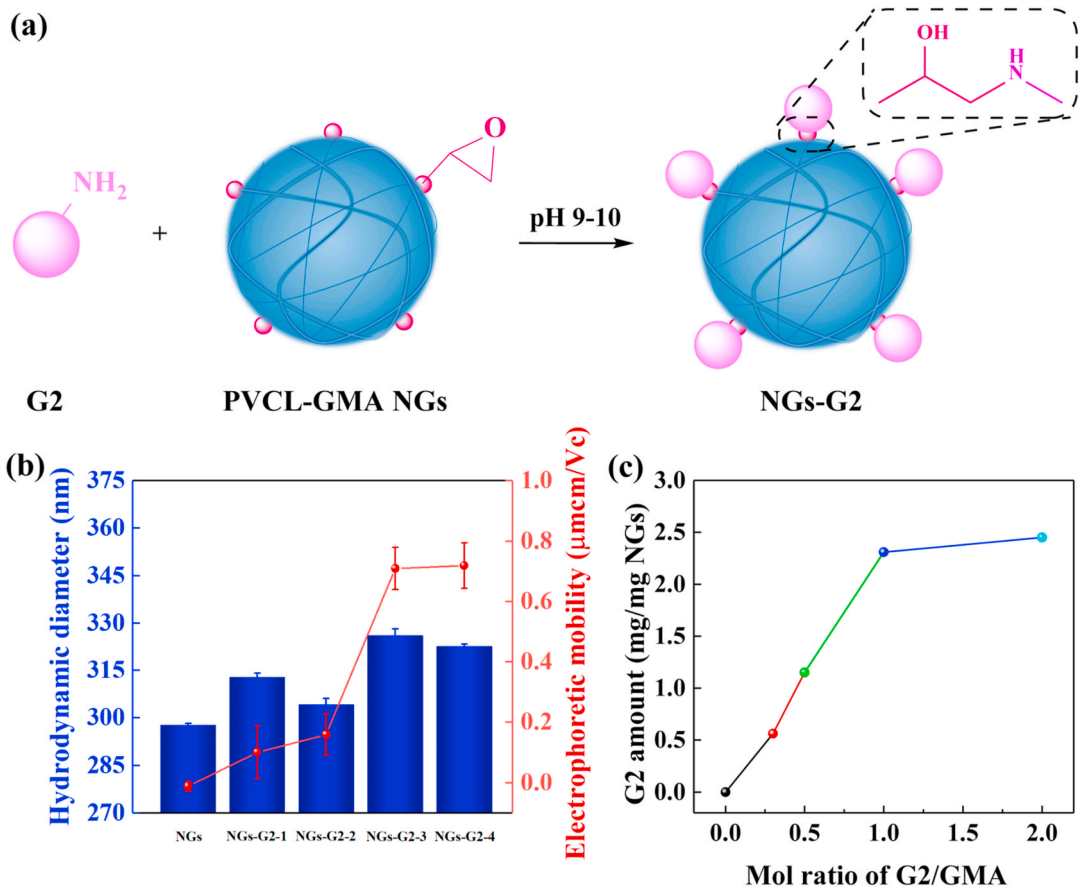

Fig. 2. (a) Schematic illustration of the synthesis of NGs-G2. (b) Hydrodynamic diameters and electrophoretic mobilities of the NGs and NGs-G2 with different G2 amounts. (c) The decorated G2 amount of NGs and NGs-G2FI at different G2/GMA molar ratios.

(2) and NGs (3) emerged uniform diameters of about 551 nm, 237 nm and 264 nm, respectively (Fig. 1d and Fig. S4). By dynamic light scattering (DLS) measurement (Fig. S5), the hydrodynamic diameters of these NGs were 622.5 nm, 292.4 nm and 336.1 nm respectively, which are bigger than that from TEM images. This is due to the swelling state of NGs in the aqueous solutions. These results indicate the size of NGs is controlled by turning the crosslinker content and surfactant concentration. For nanocarriers, the efficient tumor delivery and accumulation are attributed to the enhanced permeability and retention (EPR) effect [51]. The previous report revealed that the EPR effect typically operates in the nanocarriers with the size range of 100–400 nm [52]. Likewise, the NGs with smaller size are beneficial to tumor deep penetration [27]. Therefore, the NGs with the smallest hydrodynamic diameter (about 290 nm) will be investigated as a model system in the following experiments.

Next, the G2 dendrimer was conjugated onto the surface of NGs by the reaction of amino and epoxy groups under alkaline buffer condition (Fig. 2a). The formed NGs-G2 had higher hydrodynamic diameter than that of pristine NGs (Fig. 2b), which could be attributed to the hydrogen bonds formation between the active groups of NGs-G2 (e.g., amino, hydroxyl and carbonyl groups from G2) and water molecules. Likewise, the surface potential of NGs was neutral (−0.012 μmcm/Vc) in the simulated physiological environment of pH 7.4 buffer. For comparison,

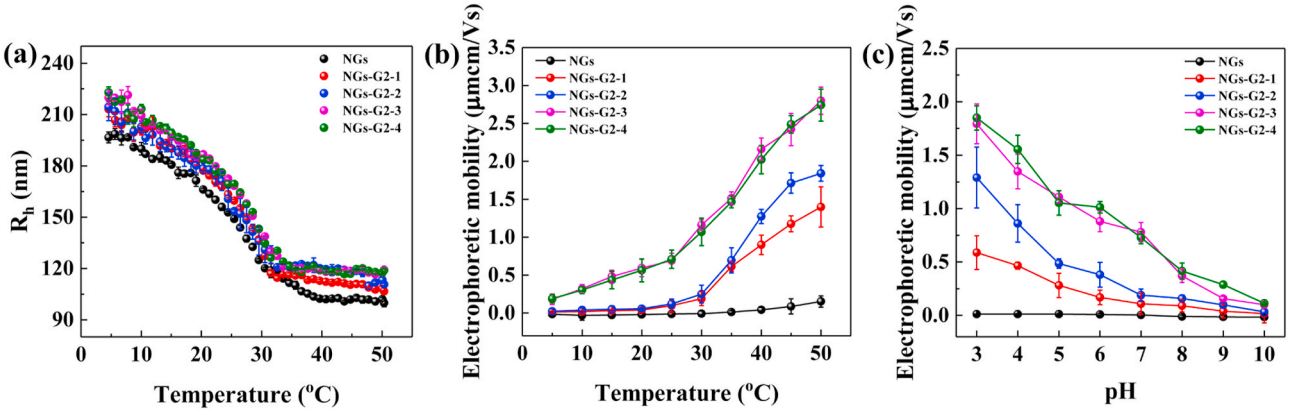

Fig. 3. (a) Hydrodynamic radiuses and (b) electrophoretic mobilities of NGs and NGs-G2 with different G2 amounts at different temperatures. (c) Electrophoretic mobilities of NGs and NGs-G2 with different G2 amounts at different pH values.

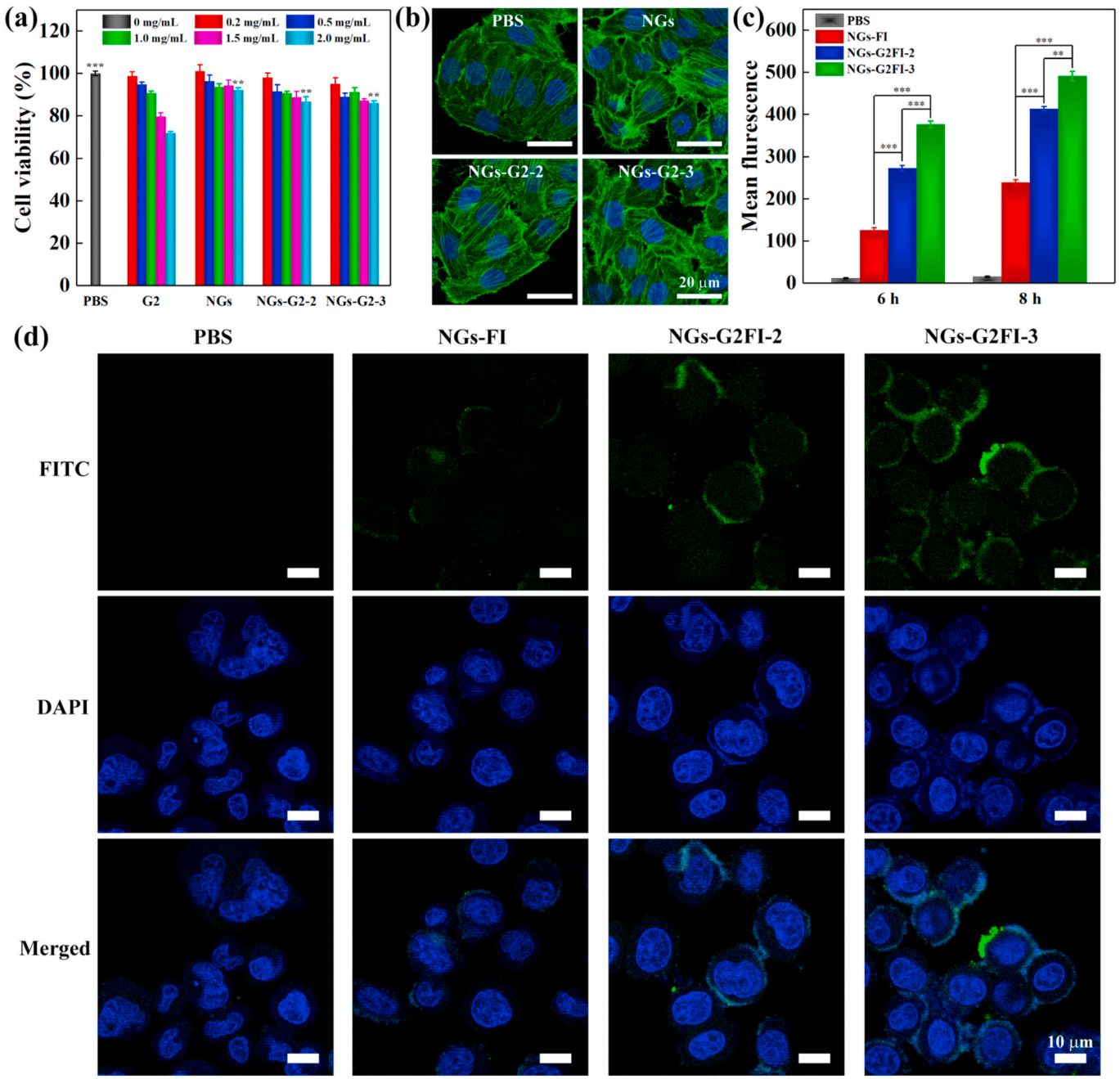

Fig. 4. (a) CCK-8 assay of SKoV3 cells treated with G2, NGs, NGs-G2-2 and NGs-G2-3 at different concentrations for 24 h. (b) CLSM images of FITC-phalloidin and DAPI stained SKoV3 cells after treated with PBS, NGs, NGs-G2-2 and NGs-G2-3 at the concentration of 1 mg/mL. (c) Flow cytometric analysis and (d) CLSM images of SKoV3 cells treated with PBS, NGs-FI, NGs-G2FI-2 and NGs-G2FI-3.

the surface potential of NGs-G2 converted to positive, and the electrophoretic mobility increased (0.101–0.7196 μmcm/Vc) with the molar ratio of G2/GMA (Fig. 2b). What's more, to visualize and quantify the decoration of G2 onto the NGs, the fluorescence labeled G2 (G2FI) was used instead of G2. Through the integration of NMR spectra (Fig. S6), the number of FI attached to each G2 was 1.9. The G2 content-dependent fluorescence intensities were explored using fluorescence microscopy (Fig. S7). With the increase of G2/GMA molar ratio, the fluorescence intensities of the NGs-G2FI enhanced significantly. Furthermore, by UV–vis analysis (Fig. 2c and Fig. S8), the quantitative G2 amount of NGs-G2FI almost reached the maximum of 2.31 mg mg^{-1} at the G2/GMA molar ratio of 1.0. The results suggest that the G2 can be coupled to the NGs, and the conjugated G2 amount reaches saturation at the G2/GMA molar ratio of 1.0.

2.2. Thermal/pH dual-responsive behaviors of NGs-G2

The thermo-responsive property of NGs-G2 with different G2 contents was validated by DLS measurement in the temperature range from 5 °C to 50 °C (Fig. 3a). The NGs displayed the VPTT of 28.4 °C. By contrast, the NGs-G2 with different G2 contents presented similar VPTT at about 28.1 °C, implying that the decoration of G2 is mainly on the surface of NGs. Moreover, at temperature above VPTT, the hydrodynamic radius of these NGs-G2 were nearly halved to about 100–120 nm due to the shrinkage of NGs. We believe that the NGs-G2 can be used as smart nanocarriers to load photothermal agents and drugs for photothermally-maneuvered drug release through the collapse of NGs. Besides, compared to NGs, the NGs-G2 exhibited a significant change of electrophoretic mobility in the temperature range 5–50 °C (Fig. 3b).

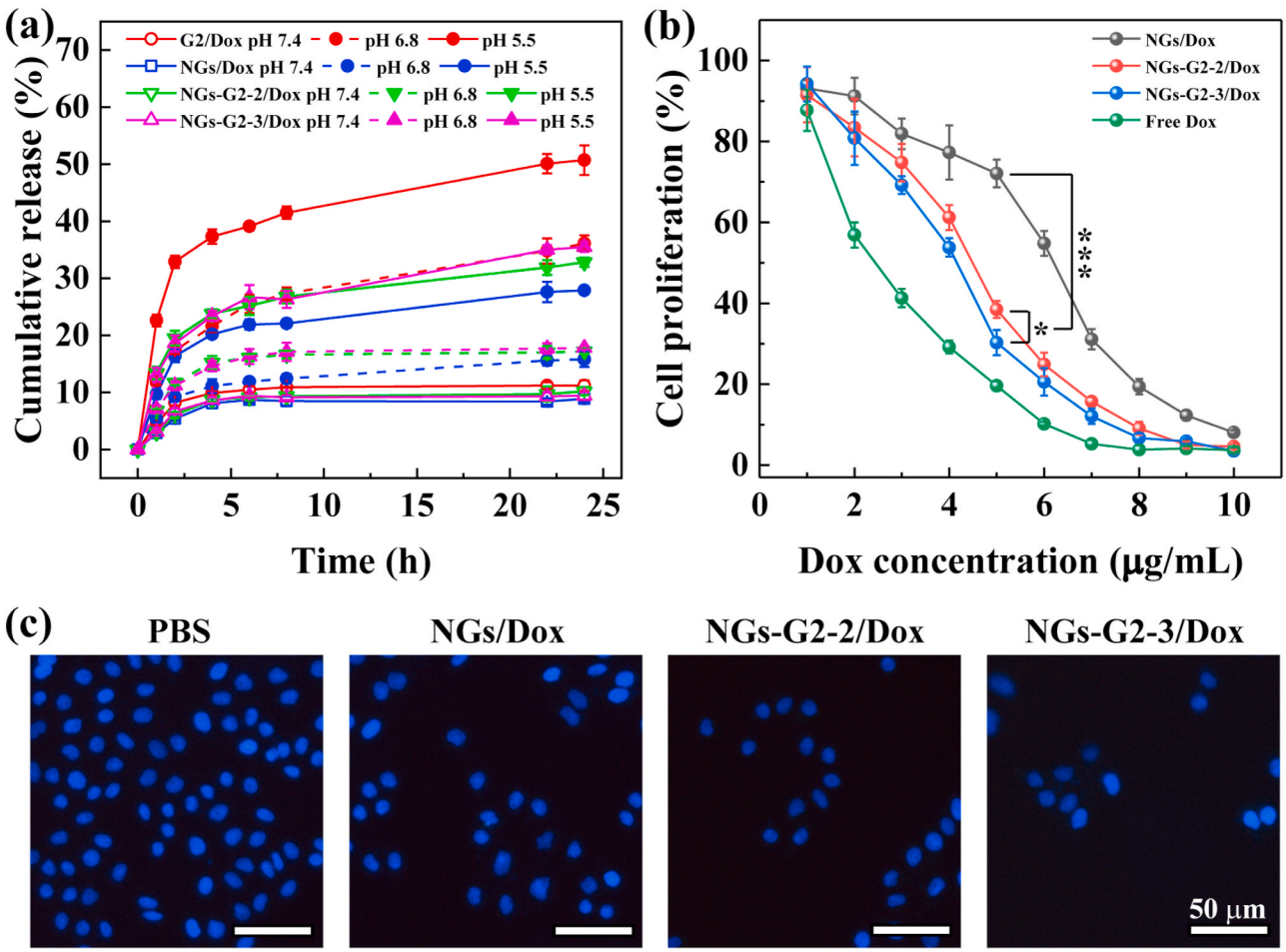

Fig. 5. (a) Dox release profile from G2/Dox, NGs/Dox, NGs-G2-2/Dox and NGs-G2-3/Dox at different pH conditions. (b) CCK-8 proliferation assay of SKoV3 cells treated with free Dox, NGs/Dox, NGs-G2-2/Dox and NGs-G2-3/Dox at different Dox concentrations for 24 h. (c) Fluorescence microscopic images of DAPI-stained SKoV3 cells treated with PBS, NGs/Dox, NGs-G2-2/Dox and NGs-G2-3/Dox for 24 h.

With the increase of temperature, the electrophoretic mobility of NGs was nearly invariant, while that of all NGs-G2 was gradually increased. This is attributed to the concentration of charges by the shrinkage of NGs-G2 outer layer [53,54].

In addition, the pH-responsive behavior of NGs-G2 was determined at the different pH values (Fig. 3c). The NGs displayed a neutral surface charge and almost unchanged electrophoretic mobility in the pH range from 10 to 3, while the positive surface charge and the increased electrophoretic mobility of NGs-G2 were observed over the whole pH range. It is due to the fact that the -NH_2 groups of NGs-G2 can acquire positive charge of H^+ and then form -NH_3^+ in the acidic environment, implying that these NGs-G2 are able to be protonated in acidic condition. The pH-responsive property of NGs-G2 can improve the cell membrane affinity, potentially enhancing the cellular internalization by cationization-mediated active transportation in the acidic cancer region.

2.3. Biocompatibility and cellular internalization

The biocompatibility of G2, NGs, NGs-G2-2 and NGs-G2-3 was assessed by CCK-8 assay (Fig. 4a). The viabilities of SKoV3 cells treated with the NGs, NGs-G2-2 and NGs-G2-3 remained above 86% in the studied concentration up to 2.0 mg/mL, while that treated with free G2 was significantly lower. Especially, under the concentration of 2.0 mg/mL, the viability of cells treated with G2 decreased to 71.8%, which is obviously lower than that treated with PBS ($p < 0.001$) or the NGs, NGs-G2-2 and NGs-G2-3 ($p < 0.05$). This indicates that G2 dendrimer exists certain toxicity at a relatively high concentration since cationic dendrimer displays strong interactions with cell membrane and can induce the membrane disruption. Contrary, the NGs-G2-2 and NGs-G2-3 retain negligible toxicity in the studied concentration range because of the biocompatible PVCL-based NGs. Furthermore, by confocal laser scanning microscopy (CLSM) imaging (Fig. 4b), the cell treated with NGs, NGs-G2-2 and NGs-G2-3 showed the integrated cytoskeleton (green) and nuclei (blue), similar to that treated with PBS.

The cellular uptake of the nanocarriers is an important parameter to evaluate their delivery property. To visualize the cellular internalization effect, the SKoV3 cells treated with NGs-FI, NGs-G2FI-2 and NGs-G2FI-3 were observed *via* the CLSM images (Fig. 4d). After co-culture for 6 h, the cells treated with NGs-G2FI-3 showed the highest fluorescence intensity when compared to that treated with NGs-FI and NGs-G2FI-2. Furthermore, the cellular internalization of NGs-FI, NGs-G2FI-2 and NGs-G2FI-3 was quantitatively tested by flow cytometric analysis (Fig. 4c and Fig. S9). All of these nanocarriers displayed time-dependent fluorescence increase in cellular uptake. After treatment for 8 h, the intracellular fluorescence intensities of NGs-G2FI-3 and NGs-G2FI-2 were 2.0 and 1.7 times higher than that of NGs-FI, respectively. This is possibly due to the fact that the cationization of NGs-G2FI in acidic cancer cell environment can facilitate cellular uptake by active transcytosis and good cell membrane affinity, while the NGs-FI are internalized by the cells by phagocytosis and passive diffusion. Overall, these results demonstrate the decoration of multivalent cooperative dendrimer on the NGs is able to elevate significantly cellular internalization.

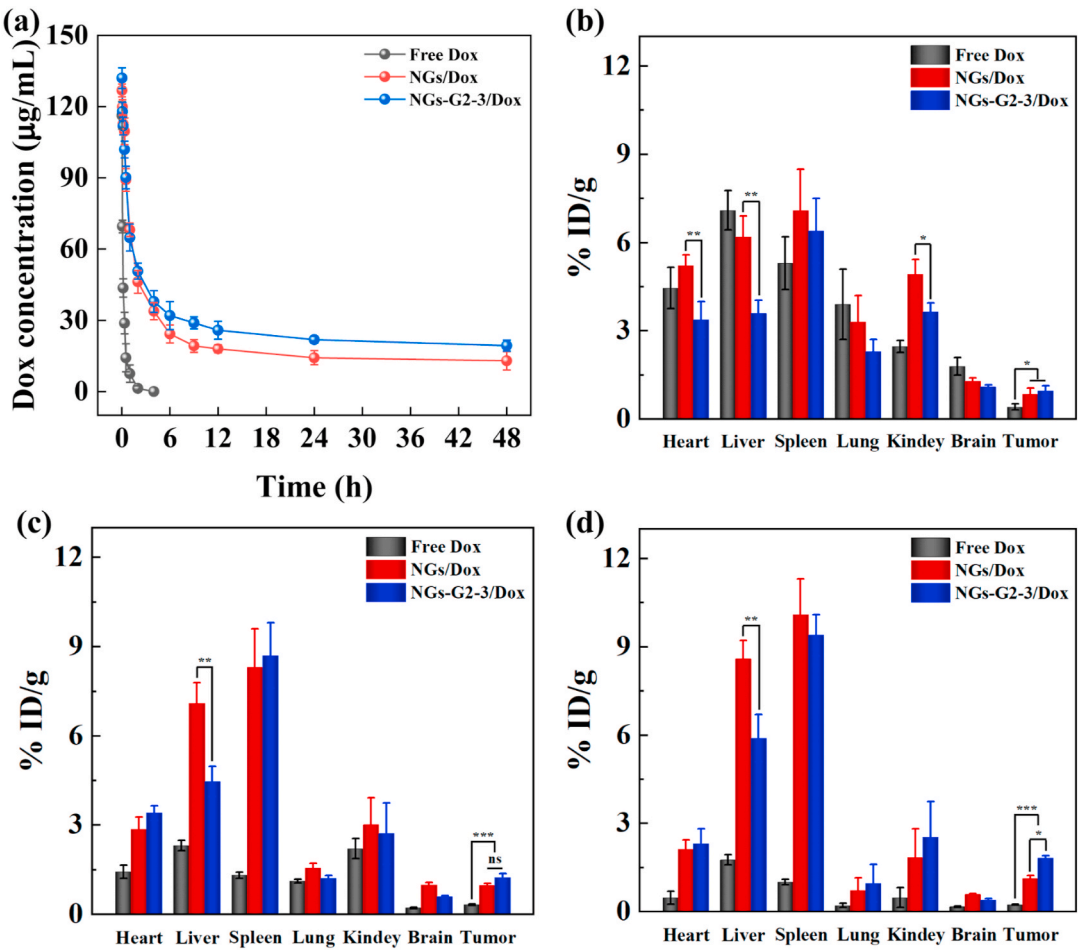

Fig. 6. (a) Pharmacokinetics of Dox after intravenous injection of free Dox, NGs/Dox, and NGs-G2-3/Dox in the mice. The biodistribution in different organs of mice bearing tumor after intravenous injection of free Dox, NGs/Dox and NGs-G2-3/Dox for (b) 3 h, (c) 12 h, and (d) 24 h.

2.4. Drug encapsulation and stimuli-responsive release

The formed nanocarriers were employed to encapsulate Dox, and the Dox loaded amounts were measured by UV–vis spectra and standard curve (Fig. S10b). After Dox loading, the Dox loaded nanocarriers emerged a typical absorption peak of Dox at 490 nm (Fig. S10a). Moreover, the hydrodynamic diameters of G2/Dox, NGs/Dox, NGs-G2-2/Dox and NGs-G2-3/Dox were 11.4 nm, 308.7 nm, 316.3 nm, 332.1 nm, and 331.7 nm, respectively. Due to the ultrasmall size, free G2 displayed the low Dox loading of 217.2 μg/mg. At the same NGs concentration, the Dox loaded amounts in NGs, NGs-G2-2 and NGs-G2-3 were about 491.4 μg/mg, 587.4 μg/mg and 613.5 μg/mg, respectively. By the calculation, the loading capacity of LC_{Dox} in the G2/Dox, NGs/Dox, NGs-G2-2/Dox and NGs-G2-3/Dox was 17.8%, 32.9%, 37.0%, and 38.0%, respectively.

Next, the drug release behaviors of these nanocarriers were investigated in PBS (pH 7.4, pH 6.8) and acetate buffer (pH 5.5) (Fig. 5a). Obviously, at pH 7.4, the Dox was slowly released in all of the nanocarriers within 24 h, and the cumulative release of these Dox loaded nanocarriers reached about 8.9%–11.2%. While the Dox was quickly released from these nanocarriers at both pH 6.8 and pH 5.5. It is remarkable that 20.2%, 23.8% and 23.4% of Dox were released from NGs/Dox, NGs-G2-2/Dox and NGs-G2-3/Dox within 4 h in pH 5.5 respectively, while a burst release of 37.3% appeared in G2/Dox at same time period that may be ascribed to the ultrasmall size of G2. Likewise, the Dox release from NGs/Dox, NGs-G2-2/Dox and NGs-G2-3/Dox was able to maintain in a sustained way and kept a constant level of Dox concentration until 24 h in the acidic condition. After 24 h, the cumulative Dox release from G2/Dox, NGs/Dox, NGs-G2-2/Dox and NGs-G2-3/Dox reached 50.7%, 27.9% 32.3% and 35.5% respectively at pH 5.5. The pH-responsive release of these Dox loaded nanocarriers is due to the proton sponge effect [46,55], that should be beneficial for inhibiting cancer cells, instead of normal tissues owing to their difference in pH value. Besides that, due to the relatively high toxicity, low loading capacity and burst release of drug, free G2 dendrimer is not suitable as a nanocarrier for drug delivery. Notably, a higher Dox release of NGs-G2-3/Dox than that of NGs/Dox was observed. This could be attributed to the fact that the protonated NGs-G2-3 with more positive charges in acidic condition are likely able to repel the positively charged Dox molecules and further promote the Dox release. These results indicate that the NGs-G2-3/Dox possess the property of pH-responsive sustained drug release, and thus may be an effective nanocarrier for the inhibition of cancer cells with long-term activity in acidic tumor regions as well as reduction baneful adverse reaction in normal tissues.

2.5. Anticancer activity in vitro

The anticancer activity of NGs/Dox, NGs-G2-2/Dox and NGs-G2-3/Dox for SKoV3 cells was evaluated by CCK-8 proliferation assay (Fig. 5b). These Dox loaded nanocarriers exhibited the concentration-dependent inhibition efficacy of cell proliferation. At the same DOX concentration, the cells treated with the NGs-G2-3/Dox displayed the lowest viability due to the improved cellular internalization and promoted drug release. Furthermore, the half maximal inhibitory concentrations (IC_{50}s) of all nanocarriers were calculated (Fig. S11), and followed the order of NGs/Dox (6.22 μg/mL) > NGs-G2-2/Dox (4.75 μg/

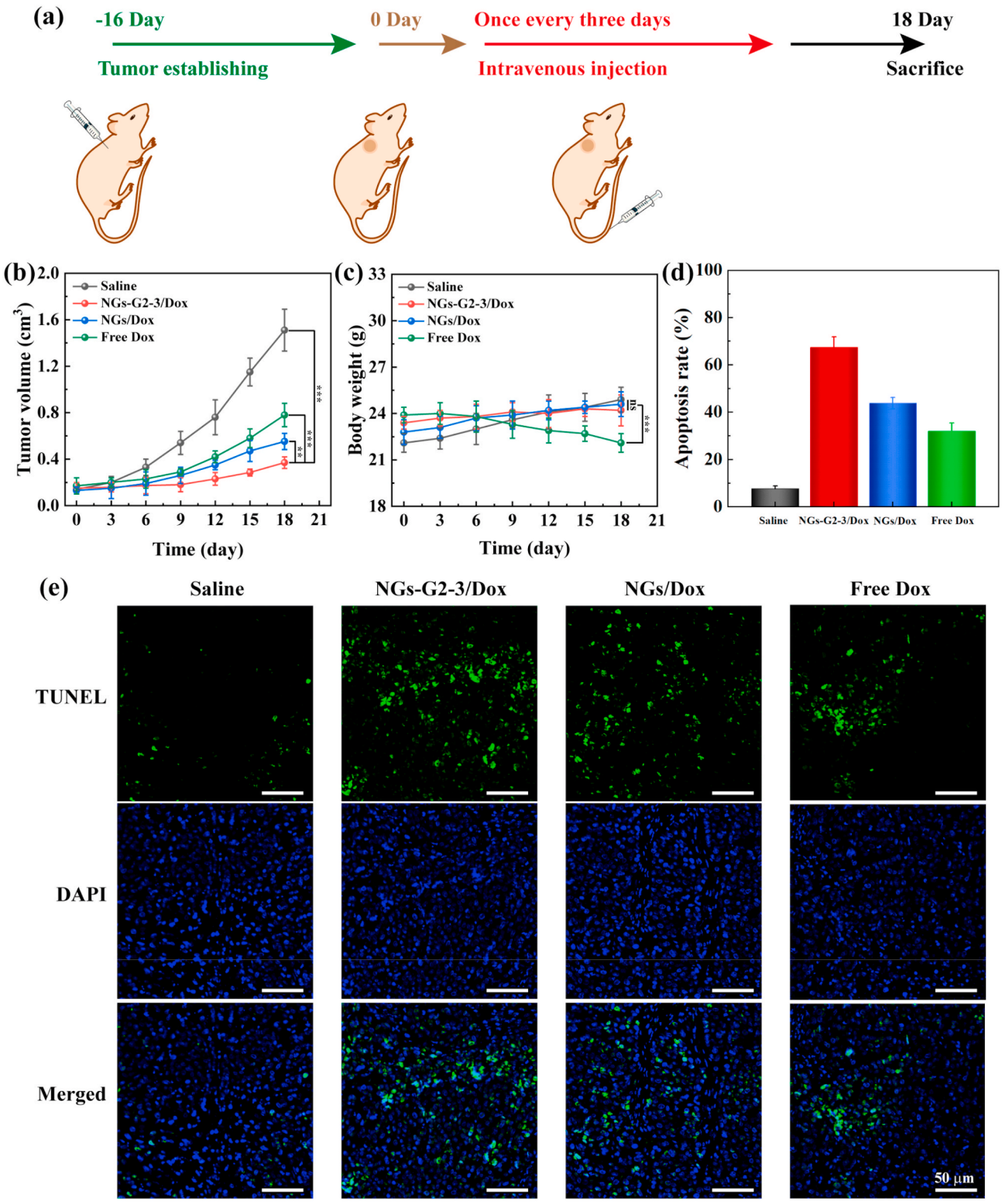

Fig. 7. (a) Schematic illustration of the administration process used for chemotherapy of tumors. (b) Tumor volume and (c) body weight of mice bearing tumor in different groups. (d) Quantitative analysis of apoptosis rate and (e) TUNEL staining of tumor sections in different groups.

mL) > NGs-G2-3/Dox (4.13 μg/mL) > Free Dox (2.59 μg/mL). Additionally, the DAPI-staining assay was performed to visually examine the enhanced anticancer activity (Fig. 5c). The cells treated with NGs-G2-3/Dox displayed the largest area of dead cells (dark regions, dead cells exfoliated from cell walls), while that treated with PBS were all alive (blue fluorescence), in agreement with the result of CCK-8 assay. These results indicate that the decoration of multivalent cooperative dendrimer onto the NGs can improve significantly the anticancer activity, and the NGs-G2-3/Dox display the most valid efficacy attributing to the sustained Dox release and enhanced cellular internalization.

2.6. Biodistribution and antitumor efficacy in vivo

To prove our original hypothesis, the discrepancies in pharmacokinetics and biodistribution of free Dox, NGs/Dox and NGs-G2-3/Dox in the mice bearing SKoV3 tumor were investigated. For pharmacokinetics, the blood Dox concentration at different time points was determined (Fig. 6a). Compared to the half-decay time ($t_{1/2}$) of free Dox (0.30 h), the NGs/Dox and NGs-G2-3/Dox displayed significantly longer $t_{1/2}$ of 5.25 h and 7.04 h, respectively. This result indicates that compared to free Dox, both NGs/Dox and NGs-G2-3/Dox can prolong blood circulation time which is beneficial for drug-load nanocarriers to be accumulated within the tumor.

Furthermore, the biodistribution of Dox in different organs was measured after intravenous injection for different time periods (Fig. 6b–d and Fig. S12). Interestingly, the liver uptake of NGs-G2-3/Dox significantly reduced when compared to that of NGs/Dox. The liver uptake reduced by 1.46–1.72 times with NGs-G2-3/Dox compared with NGs/Dox at 3–24 h post-injection. Notably, the contents of both NGs/Dox and NGs-G2-3/Dox were decreased in the major organs of heart, lung, kidney, brain at 24 h post-injection, avoiding the toxicity of long-term retention for these major organs. Different from the previous report that the nanoplatforms with positive charge prefer to accumulate in the liver [46–48], our results illustrate that the nanocarriers having overall charge nature of positively charged corona and neutral core display the reduced liver uptake. Excitingly, after intravenous injection for 12–48 h, the tumor accumulation of NGs-G2-3/Dox was relatively higher than that of NGs/Dox (Fig. 6d and Fig. S12). As a comparison, free Dox was rapidly metabolized within 24 h, and its accumulation in the tumor was significantly lower than that of both NGs/Dox and NGs-G2-3/Dox. Remarkably, these results highlight that the impact on *in vivo* biodistribution and pharmacokinetics is dependent not only on the size, surface charge, and modification, but also on the nature of the whole nanocarriers. The overall feature may affect the binding behavior of nanocarriers and proteins in body fluids, depending on the charge of both the subject and decorated surface, and hence impacting the overall biodistribution. This finding may provide a novel insight into optimizing the design, improving the biodistribution and enhancing the theranostic efficacy of nanoplatforms.

Additionally, the antitumor efficacy of NGs/Dox and NGs-G2-3/Dox was compared by the determination of tumor volume of mice bearing tumor in different groups (Saline, NGs/Dox, NGs-G2-3/Dox and free Dox). These nanocarriers were injected intravenously into mice bearing tumor in different groups respectively according to the treatment timeline (Fig. 7a). The tumors in Saline group grew rapidly, while the tumor growth inhibitory effect in NGs-G2-3/Dox group was obviously higher than that in free Dox and NGs/Dox groups (Fig. 7b and Fig. S13). Moreover, through the TUNEL staining of tumor sections in different groups (Fig. 7e), the largest area of apoptotic cells (green fluorescence) was observed in NGs-G2-3/Dox group, and the apoptotic rate of tumor region in different groups follows the order of NGs-G2-3/Dox (67.4%) > NGs/Dox (43.8%) > free Dox (31.9%) > Saline (7.7%) (Fig. 7c). The similar body weight change of the mice bearing tumor in Saline, NGs/Dox and NGs-G2-3/Dox groups revealed that the low side effects of these Dox loaded nanocarriers (Fig. 7d). In contrast, the significant reduction of body weight in Dox group indicated that free Dox exhibits side effects for mice. These results demonstrate the NGs-G2-3/Dox can indeed dramatically elevate antitumor efficacy with low side effects by the optimized biodistribution and delivery with the reduced liver accumulation, improved tumor accumulation and stimuli-responsive drug release.

3. Conclusion

In summary, we developed the dendrimer decorated NGs for enhanced antitumor efficacy of ovarian carcinoma. The PVCL-GMA NGs with tunable size were prepared using precipitation polymerization, and the NGs exhibited a unique structure that GMA-rich domains were localized on the surface of NGs. Subsequently, the G2 with different amounts was decorated on the surface of NGs by the facile strategy. The formed NGs-G2 display excellent colloidal stability in aqueous solutions, thermal/pH dual-responsive properties, good biocompatibility, improved cellular internalization, stimuli-responsive drug release, and elevated anticancer activity. More importantly, the decoration of multivalent cooperative dendrimer on the NGs renders the NGs-G2 with overall charge nature of positively charged corona and neutral core, which has a drastic effect on the beneficial biodistribution of reduced liver uptake and significantly augmented antitumor efficacy with low side effects *in vivo*. This investigation implies a new insight into nanomedicine for optimizing the design, improving the biodistribution, and enhancing the theranostic efficacy.

CRediT authorship contribution statement

Xin Li: Methodology, Software, Data curation, Writing – original draft, preparation. **Zhijun Ouyang:** Data curation, Formal analysis, Writing – original draft, preparation. **Helin Li:** Methodology, Software, Data curation. **Chaolei Hu:** Methodology, Software, Data curation. **Pabitra Saha:** Methodology, Software, Data curation. **Lingxi Xing:** Supervision, Resources, Funding acquisition, Writing – review & editing. **Xiangyang Shi:** Supervision, Resources, Funding acquisition, Writing – review & editing. **Andrij Pich:** Conceptualization, Supervision, Resources, Funding acquisition, Project administration, Writing – review & editing.

Declaration of competing interest

The authors declare that they have no known competing financial interests or personal relationships that could have appeared to influence the work reported in this paper.

Acknowledgements

This research was financially supported by the Sino-German Center for Research Promotion (GZ1505), DFG (SFB 985, Functional Microgels and Microgel Systems), National Natural Science Foundation of China (81801704 and 81761148028), Science and Technology Commission of Shanghai Municipality (18520750400), Shanghai Sailing Program (18YF1415300), and China Scholarship Council (for X. Li). The authors special thanks go to Silke Reider for STEM images.

Appendix A. Supplementary data

Supplementary data to this article can be found online at https://doi.org/10.1016/j.bioactmat.2021.02.031.

References

[1] J.J. Shi, P.W. Kantoff, R. Wooster, O.C. Farokhzad, Cancer nanomedicine: progress, challenges and opportunities, Nat. Rev. Canc. 17 (2017) 20–37.
[2] Q.X. Sun, M. Baues, B.M. Klinkhammer, J. Ehling, S. Djudjaj, N.I. Drude, C. Daniel, K. Amann, R. Kramann, H. Kim, J. Saez-Rodriguez, R. Weiskirchen, D.C. Onthank, R.M. Botnar, F. Kiessling, J. Floege, T. Lammers, P. Boor, Elastin imaging enables noninvasive staging and treatment monitoring of kidney fibrosis, Sci. Transl. Med. 11 (2019), eaat4865.
[3] Y. Matsumoto, J.W. Nichols, K. Toh, T. Nomoto, H. Cabral, Y. Miura, R.J. Christie, N. Yamada, T. Ogura, M.R. Kano, Y. Matsumura, N. Nishiyama, T. Yamasoba, Y. H. Bae, K. Kataoka, Vascular bursts enhance permeability of tumour blood vessels and improve nanoparticle delivery, Nat. Nanotechnol. 11 (2016) 533–538.
[4] P. Zhang, X.Q. Wu, G. Gardashova, Y. Yang, Y.H. Zhang, L. Xu, Y. Zeng, Molecular and functional extracellular vesicle analysis using nanopatterned microchips monitors tumor progression and metastasis, Sci. Transl. Med. 12 (2020), eaaz2878.
[5] E. Blanco, H. Shen, M. Ferrari, Principles of nanoparticle design for overcoming biological barriers to drug delivery, Nat. Biotechnol. 33 (2015) 941–951.
[6] T. Lammers, M. Ferrari, The success of nanomedicine, Nano Today 31 (2020), 100853.

[7] G.C. Jayson, E.C. Kohn, H.C. Kitchener, J.A. Ledermann, Ovarian cancer, Lancet 384 (2014) 1376–1388.

[8] A.N. Karnezis, K.R. Cho, C.B. Gilks, C.L. Pearce, D.G. Huntsman, The disparate origins of ovarian cancers: pathogenesis and prevention strategies, Nat. Rev. Canc. 17 (2017) 65–74.

[9] H.S. Choi, W.H. Liu, F.B. Liu, K. Nasr, P. Misra, M.G. Bawendi, J.V. Frangioni, Design considerations for tumour-targeted nanoparticles, Nat. Nanotechnol. 5 (2010) 42–47.

[10] X. Li, S.Y. Lu, Z.G. Xiong, Y. Hu, D. Ma, W.Q. Lou, C. Peng, M.W. Shen, X.Y. Shi, Light-addressable nanoclusters of ultrasmall iron oxide nanoparticles for enhanced and dynamic magnetic resonance imaging of arthritis, Adv. Sci. 6 (2019), 1901800.

[11] R. van der Meel, E. Sulheim, Y. Shi, F. Kiessling, W.J.M. Mulder, T. Lammers, Smart cancer nanomedicine, Nat. Nanotechnol. 14 (2019) 1007–1017.

[12] L. Ding, Z.B. Lyu, B. Louis, A. Tintaru, E. Laurini, D. Marson, M.J. Zhang, W. X. Shao, Y.F. Jiang, A. Bouhlel, L. Balasse, P. Garrigue, E. Mas, S. Giorgio, J. Iovanna, Y.Y. Huang, S. Pricl, B. Guillet, L. Peng, Surface charge of supramolecular nanosystems for in vivo biodistribution: a microSPECT/CT imaging study, Small 16 (2020), 2003290.

[13] W.H. Yuan, Z. Li, X. Xie, Z.Y. Zhang, L.M. Bian, Bisphosphonate-based nanocomposite hydrogels for biomedical applications, Bioact. Mater. 5 (2020) 819–831.

[14] A. Scotti, S. Bochenek, M. Brugnoni, M.A. Fernandez-Rodriguez, M.F. Schulte, J. E. Houston, A.P.H. Gelissen, Potemkin II, L. Isa, W. Richtering, Exploring the colloid-to-polymer transition for ultra-low crosslinked microgels from three to two dimensions, Nat. Commun. 10 (2019) 1418.

[15] G. Agrawal, R. Agrawal, Functional microgels: recent advances in their biomedical applications, Small 14 (2018), 1801724.

[16] F.A. Plamper, W. Richtering, Functional microgels and microgel systems, Acc. Chem. Res. 50 (2017) 131–140.

[17] W.J. Xu, A. Rudov, A. Oppermann, S. Wypysek, M. Kather, R. Schroeder, W. Richtering, Potemkin II, D. Woll, A. Pich, Synthesis of polyampholyte janus-like microgels by coacervation of reactive precursors in precipitation polymerization, Angew. Chem. Int. Ed. 59 (2020) 1248–1255.

[18] J.Z. Zhu, Z.C. Li, C.C. Zhang, L. Lin, S.P. Cao, H.L. Che, X.Y. Shi, H. Wang, J.C. M. van Hest, Single enzyme loaded nanoparticles for combinational ultrasound-guided focused ultrasound ablation and hypoxia-relieved chemotherapy, Theranostics 9 (2019) 8048–8060.

[19] H. Peng, X.B. Huang, A. Melle, M. Karperien, A. Pich, Redox-responsive degradable prodrug nanogels for intracellular drug delivery by crosslinking of amine-functionalized poly(N-vinylpyrrolidone) copolymers, J. Colloid Interface Sci. 540 (2019) 612–622.

[20] C.C. Zhang, W.J. Sun, Y. Wang, F. Xu, J. Qu, J.D. Xia, M.W. Shen, X.Y. Shi, Gd-/CuS-loaded functional nanogels for MR/PA imaging-guided tumor-targeted photothermal therapy, ACS Appl. Mater. Interfaces 12 (2020) 9107–9117.

[21] M.A. Al Enezy-Ulbrich, H. Malyaran, R.D. de Lange, N. Labude, R. Plum, S. Rutten, N. Terefenko, S. Wein, S. Neuss, A. Pich, Impact of reactive amphiphilic copolymers on mechanical properties and cell responses of fibrin-based hydrogels, Adv. Funct. Mater. 30 (2020), 2003528.

[22] J.Z. Zhu, T.T. Xiao, J.L. Zhang, H.L. Che, Y.X. Shi, X.Y. Shi, J.C.M. van Hest, Surface-charge-switchable nanoclusters for magnetic resonance imaging-guided and glutathione depletion-enhanced photodynamic therapy, ACS Nano 14 (2020) 11225–11237.

[23] R. Eelkema, A. Pich, Pros and cons: supramolecular or macromolecular: what is best for functional hydrogels with advanced properties? Adv. Mater. 32 (2020), 1906012.

[24] W.J. Xu, A.A. Rudov, R. Schroeder, I.V. Portnov, W. Richtering, Potemkin II, A. Pich, Distribution of ionizable groups in polyampholyte microgels controls interactions with captured proteins: from blockade and "levitation" to accelerated release, Biomacromolecules 20 (2019) 1578–1591.

[25] Y.W. Zhou, Y. Hu, W.J. Sun, S.Y. Lu, C. Cai, C. Peng, J. Yu, R. Popovtzer, M. W. Shen, X.Y. Shi, Radiotherapy-sensitized tumor photothermal ablation using gamma-polyglutamic acid nanogels loaded with polypyrrole, Biomacromolecules 19 (2018) 2034–2042.

[26] F. Xu, J.Z. Zhu, L.Z. Lin, C.C. Zhang, W.J. Sun, Y. Fan, F.F. Yin, J.C.M. van Hest, H. Wang, L.F. Du, X.Y. Shi, Multifunctional PVCL nanogels with redox-responsiveness enable enhanced MR imaging and ultrasound-promoted tumor chemotherapy, Theranostics 10 (2020) 4349–4358.

[27] C.C. Zhang, E. Gau, W.J. Sun, J.Z. Zhu, B. Schmidt, A. Pich, X.Y. Shi, Influence of size, crosslinking degree and surface structure of poly(N-vinylcaprolactam)-based microgels on their penetration into multicellular tumor spheroids, Biomater. Sci. 7 (2019) 4738–4747.

[28] W.J. Sun, S. Thies, J.L. Zhang, C. Peng, G.Y. Tang, M.W. Shen, A. Pich, X.Y. Shi, Gadolinium-loaded poly(N-vinylcaprolactam) nanogels: synthesis, characterization, and application for enhanced tumor MR imaging, ACS Appl. Mater. Interfaces 9 (2017) 3411–3418.

[29] X. Li, Z.G. Xiong, X.Y. Xu, Y. Luo, C. Peng, M.W. Shen, X.Y. Shi, Tc-99m-labeled multifunctional low-generation dendrimer-entrapped gold nanoparticles for targeted SPECT/CT dual-mode imaging of tumors, ACS Appl. Mater. Interfaces 8 (2016) 19883–19891.

[30] Y.W. Dong, T.Z. Yu, L. Ding, E. Laurini, Y.Y. Huang, M.J. Zhang, Y.H. Weng, S. T. Lin, P. Chen, D. Marson, Y.F. Jiang, S. Giorgio, S. Pricl, X.X. Liu, P. Rocchi, L. Peng, A dual targeting dendrimer-mediated siRNA delivery system for effective gene silencing in cancer therapy, J. Am. Chem. Soc. 140 (2018) 16264–16274.

[31] S.Y. Lu, X. Li, J.L. Zhang, C. Peng, M.W. Shen, X.Y. Shi, Dendrimer-stabilized gold nanoflowers embedded with ultrasmall iron oxide nanoparticles for multimode imaging-guided combination therapy of tumors, Adv. Sci. 5 (2018), 1801612.

[32] L. Ding, Z.B. Lyu, A. Tintaru, E. Laurini, D. Marson, B. Louis, A. Bouhlel, L. Balasse, S. Fernandez, P. Garrigue, E. Mas, S. Giorgio, S. Pricl, B. Guillet, L. Peng, A self-assembling amphiphilic dendrimer nanotracer for SPECT imaging, Chem. Commun. 56 (2020) 301–304.

[33] H.J. Li, J.Z. Du, X.J. Du, C.F. Xu, C.Y. Sun, H.X. Wang, Z.T. Cao, X.Z. Yang, Y. H. Zhu, S.M. Nie, J. Wang, Stimuli-responsive clustered nanoparticles for improved tumor penetration and therapeutic efficacy, Proc. Natl. Acad. Sci. U.S.A. 113 (2016) 4164–4169.

[34] S. Mignani, X.Y. Shi, M. Zablocka, J.P. Majoral, Dendrimer-enabled therapeutic antisense delivery systems as innovation in medicine, Bioconjugate Chem. 30 (2019) 1938–1950.

[35] S. Mignani, J. Rodrigues, H. Tomas, R. Roy, X.Y. Shi, J.P. Majoral, Bench-to-bedside translation of dendrimers: reality or utopia? A concise analysis, Adv. Drug Deliv. Rev. 136 (2018) 73–81.

[36] C. Song, M.W. Shen, J. Rodrigues, S. Mignani, J.P. Majoral, X.Y. Shi, Superstructured poly(amidoamine) dendrimer-based nanoconstructs as platforms for cancer nanomedicine: a concise review, Coord. Chem. Rev. 421 (2020), 213463.

[37] B. Wang, S. Van Herck, Y. Chen, X.Y. Bai, Z.F. Zhong, K. Deswarte, B.N. Lambrecht, N.N. Sanders, S. Lienenklaus, H.W. Scheeren, S.A. David, F. Kiessling, T. Lammers, B.G. De Geest, Y. Shi, Potent and prolonged innate immune activation by enzyme-responsive imidazoquinoline TLR7/8 agonist prodrug vesicles, J. Am. Chem. Soc. 142 (2020) 12133–12139.

[38] M.J. Xuan, J.X. Shao, J.B. Li, Cell membrane-covered nanoparticles as biomaterials, Natl. Sci. Rev. 6 (2019) 551–561.

[39] Y.L. Li, D. Maciel, J. Rodrigues, X.Y. Shi, H. Tomas, Biodegradable polymer nanogels for drug/nucleic acid delivery, Chem. Rev. 115 (2015) 8564–8608.

[40] O.U. Akakuru, M.Z. Iqbal, C. Liu, J. Xing, Z.N. Wei, Z.Q. Jiang, Q.L. Fang, B. Yuan, E.I. Nosike, J.B. Xia, Y.H. Jin, J.J. Zheng, A.G. Wu, Self-assembled, biocompatible and biodegradable TEMPO-conjugated nanoparticles enable folate-targeted tumor magnetic resonance imaging, Appl. Mater. Today 18 (2020), 100524.

[41] M.K. Khang, J. Zhou, C.M. Co, S.X. Li, L.P. Tang, A pretargeting nanoplatform for imaging and enhancing anti-inflammatory drug delivery, Bioact. Mater. 5 (2020) 1102–1112.

[42] Q. Zhou, S.Q. Shao, J.Q. Wang, C.H. Xu, J.J. Xiang, Y. Piao, Z.X. Zhou, Q.S. Yu, J. B. Tang, X.R. Liu, Z.H. Gan, R. Mo, Z. Gu, Y.Q. Shen, Enzyme-activatable polymer-drug conjugate augments tumour penetration and treatment efficacy, Nat. Nanotechnol. 14 (2019) 799–809.

[43] G.W. Wang, Z.X. Zhou, Z.H. Zhao, Q.Y. Li, Y.L. Wu, S. Yan, Y.Q. Shen, P.T. Huang, Enzyme-triggered transcytosis of dendrimer-drug conjugate for deep penetration into pancreatic tumors, ACS Nano 14 (2020) 4890–4904.

[44] S. Sindhwani, A.M. Syed, J. Ngai, B.R. Kingston, L. Maiorino, J. Rothschild, P. MacMillan, Y.W. Zhang, N.U. Rajesh, T. Hoang, J.L.Y. Wu, S. Wilhelm, A. Zilman, S. Gadde, A. Sulaiman, B. Ouyang, Z. Lin, L.S. Wang, M. Egeblad, W.C. W. Chan, The entry of nanoparticles into solid tumours, Nat. Mater. 19 (2020) 566–575.

[45] M. Goncalves, D. Maciel, D. Capelo, S.L. Xiao, W.J. Sun, X.Y. Shi, J. Rodrigues, H. Tomas, Y.L. Li, Dendrimer-assisted formation of fluorescent nanogels for drug delivery and intracellular imaging, Biomacromolecules 15 (2014) 492–499.

[46] X. Li, L.X. Xing, Y. Hu, Z.J. Xiong, R.Z. Wang, X.Y. Xu, L.F. Du, M.W. Shen, X.Y. Shi, An RGD-modified hollow silica@Au core/shell nanoplatform for tumor combination therapy, Acta Biomater. 62 (2017) 273–283.

[47] E.K.H. Chow, D. Ho, Cancer nanomedicine: from drug delivery to imaging, Sci. Transl. Med. 5 (2013), 216rv214.

[48] H.M. Chen, W.Z. Zhang, G.Z. Zhu, J. Xie, X.Y. Chen, Rethinking cancer nanotheranostics, Nat. Rev. Mater. 2 (2017), 17024.

[49] X. Li, L.X. Xing, K.L. Zheng, P. Wei, L.F. Du, M.W. Shen, X.Y. Shi, Formation of gold nanostar-coated hollow mesoporous silica for tumor multimodality imaging and photothermal therapy, ACS Appl. Mater. Interfaces 9 (2017) 5817–5827.

[50] E. Gau, D.M. Mate, Z. Zou, A. Oppermann, A. Topel, F. Jakob, D. Woll, U. Schwaneberg, A. Pich, Sortase-mediated surface functionalization of stimuli-responsive microgels, Biomacromolecules 18 (2017) 2789–2798.

[51] Y. Nakamura, A. Mochida, P.L. Choyke, H. Kobayashi, Nanodrug delivery: is the enhanced permeability and retention effect sufficient for curing cancer? Bioconjugate Chem. 27 (2016) 2225–2238.

[52] R. Bawa, Bio-nanotechnology: A Revolution in Food, Biomedical and Health Science, Wiley-Blackwell, 2013, pp. 720–732.

[53] X. Fu, L. Hosta-Rigau, R. Chandrawati, J.W. Cui, Multi-stimuli-responsive polymer particles, films, and hydrogels for drug delivery, Inside Chem. 4 (2018) 2084–2107.

[54] H. Kim, K. Kim, S.J. Lee, Nature-inspired thermo-responsive multifunctional membrane adaptively hybridized with PNIPAm and PPy, NPG Asia Mater. 9 (2017), e445.

[55] Y.J. Liu, P. Bhattarai, Z.F. Dai, X.Y. Chen, Photothermal therapy and photoacoustic imaging via nanotheranostics in fighting cancer, Chem. Soc. Rev. 48 (2019) 2053–2108.